*Supporting Information*

# Determinants of Reactivity and Selectivity in Soluble Epoxide Hydrolase from QM/MM Modeling

*Richard Lonsdale, Simon Hoyle, Daniel T. Grey, Lars Ridder and Adrian J. Mulholland*

Centre for Computational Chemistry, School of Chemistry, University of Bristol, Cantock's Close, Bristol, BS8 1TS, UK, and Netherlands eScience Center, Science Park 140, 1098 XG Amsterdam, The Netherlands.

Adrian.Mulholland@bristol.ac.uk

Phone: +44 (0) 117 928 9097 Fax: +44 (0) 117 925 0612

**Part A: Full reference for references [34] and [34]**

[34] - MacKerell, A. D.; Bashford, D.; Bellott, M.; Dunbrack, R. L.; Evanseck, J. D.; Field, M. J.; Fischer, S.; Gao, J.; Guo, H.; Ha, S.; Joseph-McCarthy, D.; Kuchnir, L.; Kuczera, K.; Lau, F. T. K.; Mattos, C.; Michnick, S.; Ngo, T.; Nguyen, D. T.; Prodhom, B.; Reiher, W. E.; Roux, B.; Schlenkrich, M.; Smith, J. C.; Stote, R.; Straub, J.; Watanabe, M.; Wiorkiewicz-Kuczera, J.; Yin, D.; Karplus, M. *J. Phys. Chem. B* **1998**, *102*, 3586.

[44] - H.-J. Werner, P. J. Knowles, F. R. Manby, M. Schütz, P. Celani, G. Knizia, T. Korona, R. Lindh, A. Mitrushenkov, G. Rauhut, T. B. Adler, R. D. Amos, A. Bernhardsson, A. Berning, D. L. Cooper, M. J. O. Deegan, A. J. Dobbyn, F. Eckert, E. Goll, C. Hampel, A. Hesselmann, G. Hetzer, T. Hrenar, G. Jansen, C. Köppl, Y. Liu, A. W. Lloyd, R. A. Mata, A. J. May, S. J. McNicholas, W. Meyer, M. E. Mura, A. Nicklaß, P. Palmieri, K. Pflüger, R. Pitzer, M. Reiher, T. Shiozaki, H. Stoll, A. J. Stone, R. Tarroni, T. Thorsteinsson, M. Wang, A. Wolf; MOLPRO, 2006.1 ed.; University College Cardiff Consultants Limited; Cardiff, UK, 2004.

**Part B: Detailed setup procedure for the AM1/CHARMM umbrella sampling molecular dynamics simulations.**

Hydrogen atoms were added to the crystal structure coordinates using the HBUILD routine in CHARMM. Each system was put through 500 steps of steepest descent (SD) minimisation with everything but the substrate constrained. A further 500 steps of adapted basis Newton Raphson (ABNR) minimisation was applied, with everything but the substrate and Asp333 side chain constrained. The system was solvated by superimposing a 23.3 Å radius sphere of pre-equilibrated TIP3P water molecules. All water molecules either outside an 18 Å sphere from the Cγ atom of Asp333 or with an oxygen atom within 2.6 Å of another heavy atom were removed. Two different models of the truncated sEH were created: one with His523 protonated at the Nε atom and one without a protonated Nε group. A deformable boundary potential of radius 19.8 Å was applied to prevent water molecules evaporating from the solvent surface. The SHAKE algorithm was used to fix the length of all MM bonds involving a hydrogen atom. 500 steps of SD minimisation were applied with everything but the water molecules restrained. A frictional coefficient of 62 $ps^{-1}$ was applied to the oxygen atoms of the water molecules. The water molecules were then equilibrated with 5 ps of stochastic boundary MD at 300 K. Any water molecules that had moved further than 18 Å from the Asp333 Cγ atom were deleted.

Stochastic boundary conditions were used in all MD simulations. The reaction region was defined as a 14 Å radius sphere centered on the Asp333 Cγ atom and modelled using Newtonian dynamics. The buffer region was defined as the region beyond this 14Å sphere and was split into three sections of radius 1 Å and a fourth that contained the remaining atoms. Harmonic restraints were applied to atoms in the buffer region with force constants increasing in value (from 0.22 to 1.7 kcal $mol^{-1}$ $Å^{-2}$) according to their distance from the center. The buffer region was simulated using Langevin dynamics. A further 5000 steps of ABNR minimisation was applied to each system.

Each sEH-substrate complex was put through a stochastic boundary MD simulation in order to

equilibrate the sEH-substrate systems. A frictional coefficient of 250ps$^{-1}$ was applied to all non-hydrogen atoms excluding water molecules, which were treated with a frictional coefficient of 62ps$^{-1}$. The SHAKE algorithm was applied to all bonds involving hydrogen atoms outside of the QM region and a time step of 1fs was used. Non-bonded interactions were calculated within a 13Å cut-off distance. QM/MM electrostatic interactions were scaled down using a switching function between 10 and 14 Å. The non-bonded list was updated every 25 steps. Each equilibration simulation consisted of 15ps of stochastic boundary (SB) dynamics. Ten simulations of each sEH-substrate complex were performed with different ISEED numbers, resulting in ten different starting structures of sEH and each substrate as starting points for the umbrella sampling simulations. Coordinates were saved every 10ps.

In some cases, a restraint to the epoxide C—H bonds was required. This was due to migration of a proton from the adjacent carbon to the epoxide carbon undergoing attack, resulting in free energy profiles tending to infinity. This restraint was harmonic, with a force constant of 100kcal mol$^{-1}$ Å$^{-2}$ and an equilibrium bond length of 1.5 Å. To confirm that the restraint did not affect the free energy barriers the same restraint was applied to simulations that had already been run successfully. It was found that the additional restraint had no effect on the barriers.

**Part C: Additional details of setup procedure for the AM1/CHARMM22 potential energy calculations.**

TS structures taken from the MD simulations were used as initial structures for AM1/CHARMM optimisations. Each optimisation consisted of 1000 steps of ABNR minimisation to give a RMS gradient of 0.0001 kcal mol⁻¹ Å⁻¹. The reaction coordinate was restrained using a force constant of 1000kcal $mol^{-1}$ $Å^{-1}$.

**Part D: Free energy barriers, $\Delta G^{\ddagger}$ [in kcal/mol], from preliminary AM1/CHARMM22 umbrella sampling MD simulations. 'P' denotes simulations with a protonated His523, 'N' denotes simulations with a neutral His523;**

| | $\Delta G^{\ddagger}$ (**P**) | | | | | |
|---|---|---|---|---|---|---|
| | t-SO | | t-DPPO(1) | | t-DPPO(2) | |
| Pathway | C(1) | C(2) | C(1) | C(2) | C(1) | C(2) |
| a | 18.4 | 33.5 | 22.7 | 24.2 | 17.6 | 27.5 |
| b | 23.5 | 32.8 | 20.8 | 24.9 | 19.2 | 25.2 |
| c | 19.3 | 36.2 | 25.5 | 24.3 | 16.4 | 25.3 |
| d | 20.5 | 33.3 | 19.9 | 24.4 | 17.9 | 29.8 |
| e | 22.7 | 34.4 | 19.2 | 23.2 | 18.4 | 25.3 |
| Average | 20.9 | 34.0 | 21.6 | 24.2 | 17.9 | 26.6 |

| | $\Delta G\ddagger$ (**N**) | | | | | |
|---|---|---|---|---|---|---|
| | t-SO | | t-DPPO(1) | | t-DPPO(2) | |
| Pathway | C(1) | C(2) | C(1) | C(2) | C(1) | C(2) |
| a | 30.3 | 32.7 | 30.4 | 25.7 | 32.8 | 37.4 |
| b | 32.6 | 31.4 | 29.6 | 27.1 | 27.7 | 35.7 |
| c | 35.7 | 31.5 | 29.4 | 29.1 | 30.9 | 30.8 |
| d | 33.3 | 32.7 | 29.1 | 28.4 | 25.3 | 30.5 |
| e | 35.3 | 32.1 | 21.4 | 25.3 | 30.2 | 31.8 |

| | | | | | | |
|---|---|---|---|---|---|---|
| Average | 33.4 | 32.1 | 28.0 | 27.1 | 29.4 | 33.2 |

**Part E: Free energy barriers, $\Delta G^{\ddagger}$ [in kcal/mol], from extended AM1/CHARMM22 umbrella sampling MD simulations.**

| | $\Delta G^{\ddagger}$ (**P**) | | | | | |
|---|---|---|---|---|---|---|
| | t-SO | | t-DPPO(1) | | t-DPPO(2) | |
| Pathway | C(1) | C(2) | C(1) | C(2) | C(1) | C(2) |
| a | 23.7 | 28.8 | 19.4 | 25.5 | 24.8 | 31.0 |
| b | 18.9 | 32.0 | 19.2 | 25.7 | 24.8 | 31.5 |
| c | 22.2 | 28.0 | 18.8 | 23.0 | 24.5 | 29.0 |
| d | 22.9 | * | 18.9 | 25.5 | 23.9 | 33.3 |
| e | 18.4 | 29.9 | 19.1 | 23.8 | 21.6 | 29.1 |
| f | 23.6 | 29.7 | 18.9 | 26.0 | 19.3 | 31.4 |
| g | 24.8 | 30.0 | 19.0 | 23.8 | 28.8 | * |
| h | 21.5 | 29.2 | 19.5 | 24.8 | 22.1 | 26.5 |
| i | 24.5 | 29.1 | 19.2 | 24.6 | 19.8 | 30.5 |
| j | 24.2 | 29.9 | 19.3 | * | 20.0 | * |
| Average | 22.5 | 29.6 | 19.1 | 24.7 | 22.9 | 30.3 |

* denotes profiles that did not converge

**Part F: Potential energy barriers, $\Delta E^{\ddagger}$ [in kcal/mol], calculated at the AM1/CHARMM22 level**

| | $\Delta E^{\ddagger}$ (**P**) | | | | | |
|---|---|---|---|---|---|---|
| | t-SO | | t-DPPO(1) | | t-DPPO(2) | |
| Pathway | C(1) | C(2) | C(1) | C(2) | C(1) | C(2) |
| a | 20.5 | 27.8 | 19.0 | 17.6 | 26.1 | 32.6 |
| b | 16.7 | * | 18.1 | 20.9 | 26.1 | 32.4 |
| c | 17.5 | 27.4 | 21.2 | 18.9 | 16.9 | * |
| d | 14.8 | * | 19.7 | 18.7 | 16.8 | 34.8 |
| e | 15.8 | 27.0 | 19.4 | 22.6 | 16.8 | 25.9 |
| f | 25.8 | 30.3 | 20.0 | 17.7 | 16.4 | 34.5 |
| g | 21.2 | * | 20.7 | 17.6 | 28.1 | * |
| h | 21.3 | * | 19.7 | 18.7 | 20.1 | 34.5 |
| i | 12.8 | * | 20.7 | 19.9 | 15.4 | 31.9 |
| j | 23.0 | 27.8 | 19.9 | * | 17.4 | * |
| Average | 18.9 | 28.1 | 19.8 | 19.2 | 20.0 | 32.4 |
| Boltzmann average | 14.2 | 27.6 | 19.2 | 18.2 | 16.5 | 27.1 |

* denotes profiles that did not converge

**Part G: Potential energy barriers calculated with higher levels of QM theory**

**G1: Potential energy barriers, $\Delta E^{\ddagger}$ [in kcal/mol], calculated at the B3LYP-6-31G(d)/CHARMM22 level. Barriers from single point energy calculations at the B3LYP-6-311+G(d,p)// B3LYP-6-31G(d)/CHARMM22 level are given in parentheses.**

| | $\Delta E^{\ddagger}$ (**P**) | | | | | |
|---|---|---|---|---|---|---|
| | t-SO | | t-DPPO(1) | | t-DPPO(2) | |
| Pathway | C(1) | C(2) | C(1) | C(2) | C(1) | C(2) |
| a | 6.9 (6.5) | 14.8 (14.6) | 6.7 | 10.5 (9.7) | 9.2 | 11.2 |
| b | 5.5 | * | 10.4 | 12.7 | 9.2 | 20.0 |
| c | 8.5 | 18.3 | 10.4 | 10.5 | 7.9 | 14.9 |
| d | 5.7 | * | 9.4 (8.9) | 11.6 | 6.7 | 19.2 |
| e | 4.7 | 18.1 | 9.2 | 8.0 | 5.0 | 14.4 |
| f | 11.2 | 17.2 | 8.4 | 10.5 | 4.6 | 15.4 (15.6) |
| g | 10.3 | 15.1 | 8.1 | 10.5 | 10.3 | * |
| h | 11.0 | * | 7.8 | 11.4 | 7.0 (7.2) | 11.5 |
| i | 4.8 | * | 8.8 | 9.4 | 4.5 | 15.9 |
| j | 10.7 | 13.9 | 9.4 | * | 4.1 | * |
| Average | 7.9 | 16.7 | 8.9 | 10.6 | 6.9 | 15.3 |
| Boltzmann average | 5.6 | 14.8 | 7.9 | 9.2 | 5.0 | 12.2 |

* denotes profiles that did not converge

**G2: Dependence of the potential energy barrier, $\Delta E^{\ddagger}$ [in kcal/mol], on the choice of DFT functional. Profiles were fully optimized at the DFT/CHARMM22 level with each functional (F) for the 'a' nucleophilic ring opening pathway of t-SO.**

| | $\Delta E^{\ddagger}$ (**P**) | |
|---|---|---|
| F | C(1) | C(2) |
| B3LYP/6-31G(d) | 6.9 | 14.8 |
| BP86/6-31G(d) | 6.1 | 12.3 |
| BHandHLYP/6-31G(d) | 11.2 | 21.1 |

**Part H: Gas phase single point energies calculated on the B3LYP/6-31G(d)/CHARMM22 QM structures geometries from the 'a' pathway for the t-SO model. $E_{RC}$ and $E_{TS}$ correspond to the absolute energies [in Hartrees] of the reactant complex and transition states respectively. $\Delta E^{\ddagger}$ corresponds to the potential energy barrier [in kcal/mol]. Energies are calculated at the B3LYP/6-31G(d) level of theory. The Poisson Boltzmann solvation model in Jaguar was used, with a dielectric constant of 80.37 and probe radius of 1.40 Å.**

| | | C(1) | C(2) |
|---|---|---|---|
| QM Only | $E_{RC}$ | -844.4194181 | -844.4211038 |
| | $E_{TS}$ | -844.395994 | -844.3927297 |
| | $\Delta E^{\ddagger}$ | 14.7 | 17.8 |
| QM + Solvation | $E_{RC}$ | -844.6368053 | -844.6387378 |
| | $E_{TS}$ | -844.6121079 | -844.606066 |
| | $\Delta E^{\ddagger}$ | 15.5 | 20.5 |

**Part I: SCS-MP2/CHARMM22 potential energy barriers, $\Delta E^{\ddagger}$ [in kcal/mol], calculated as single point energies on the B3LYP-6-31G(d)/CHARMM22 structures. The cc-pVTZ basis set was used, with additional diffuse functions added to the epoxide oxygen atom.**

| | $\Delta E^{\ddagger}$ (**P**) | | | | | |
|---|---|---|---|---|---|---|
| | t-SO | | t-DPPO(1) | | t-DPPO(2) | |
| Pathway | C(1) | C(2) | C(1) | C(2) | C(1) | C(2) |
| a | 10.6 | 18.2 | - | 14.0 | - | - |
| d | - | - | 11.0 | - | - | - |
| f | - | - | - | - | - | 20.0 |
| h | - | - | - | - | 11.4 | - |

## Part K: Additional hydrogen bond information

**K1: Hydrogen bonding to epoxide oxygen in extended AM1/CHARMM22 umbrella sampling MD simulations of ring opening at C(1) of t-SO (pathway 'a'):**

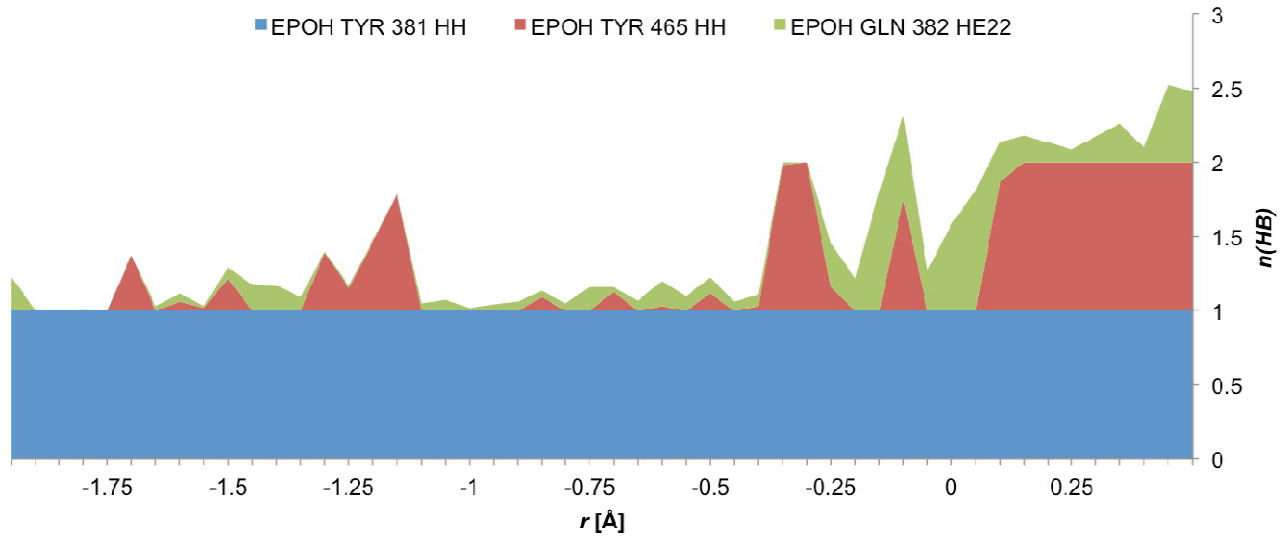


**K2: Hydrogen bonding to epoxide oxygen in extended AM1/CHARMM22 umbrella sampling MD simulations of ring opening at C(1) of t-SO (pathway 'b'):**

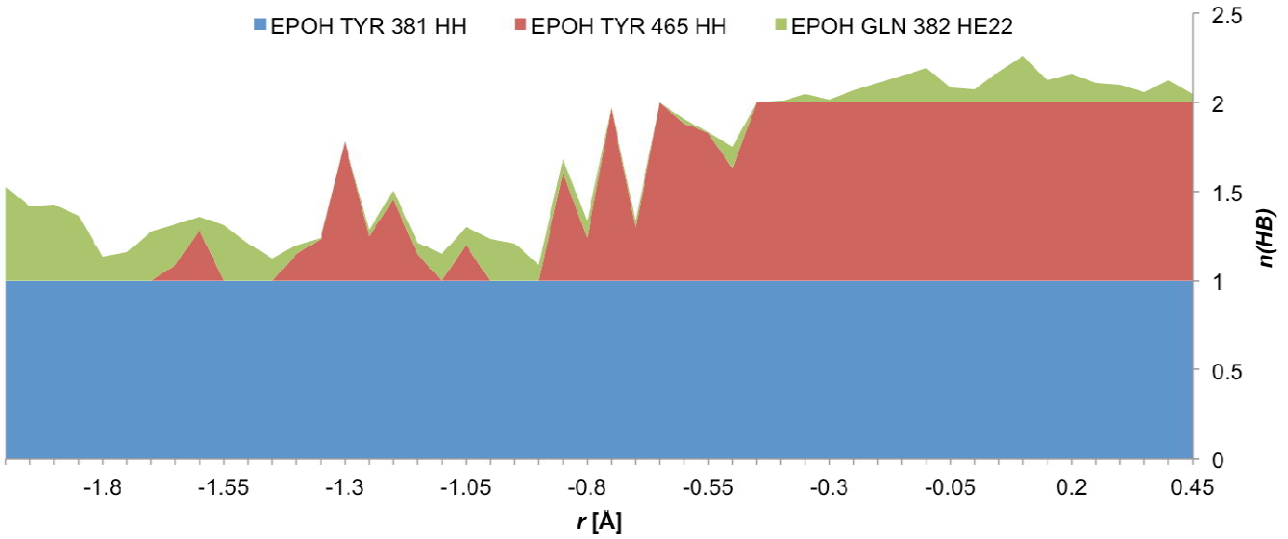

**K3: Hydrogen bonding to epoxide oxygen in extended AM1/CHARMM22 umbrella sampling MD simulations of ring opening at C(1) of t-SO (pathway 'c'):**

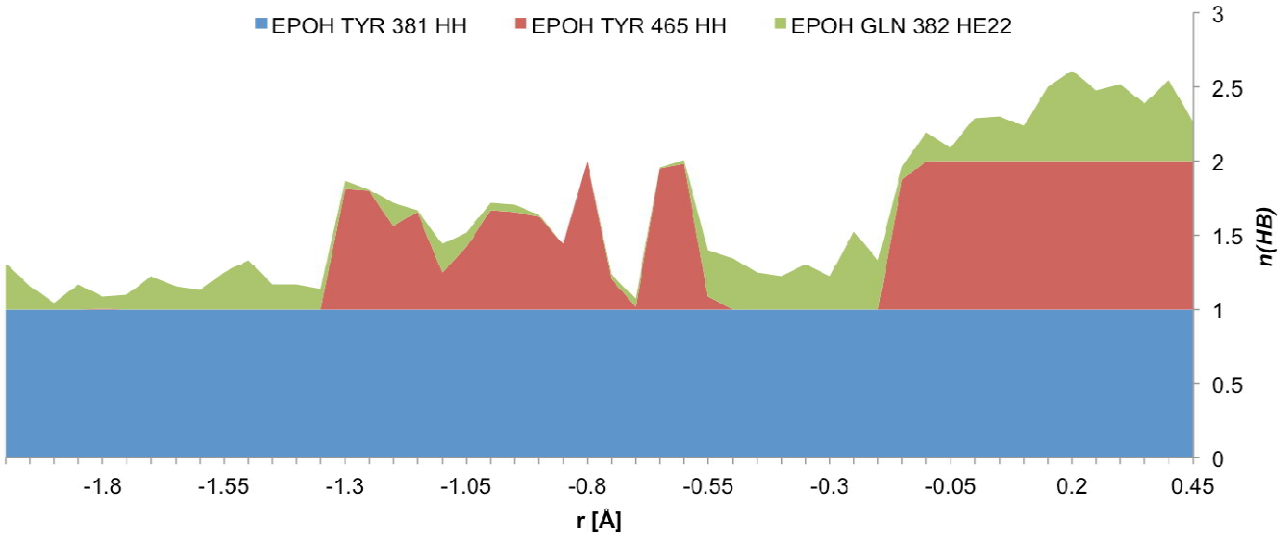


**K4: Hydrogen bonding to epoxide oxygen in extended AM1/CHARMM22 umbrella sampling MD simulations of ring opening at C(1) of t-SO (pathway 'd'):**

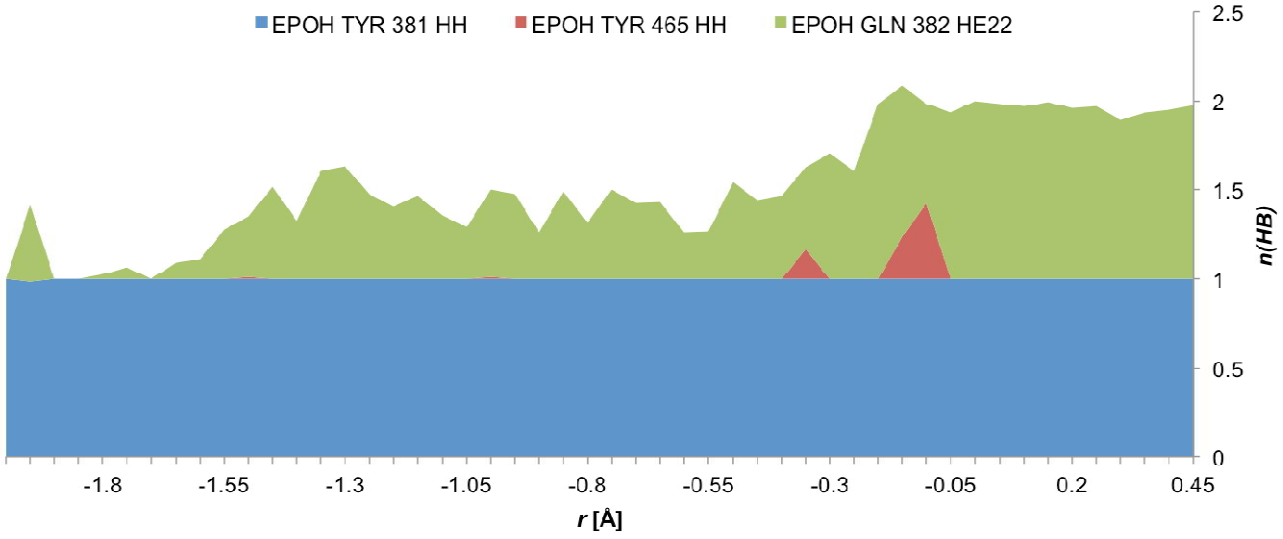

**K5: Hydrogen bonding to epoxide oxygen in extended AM1/CHARMM22 umbrella sampling MD simulations of ring opening at C(1) of t-SO (pathway 'e'):**

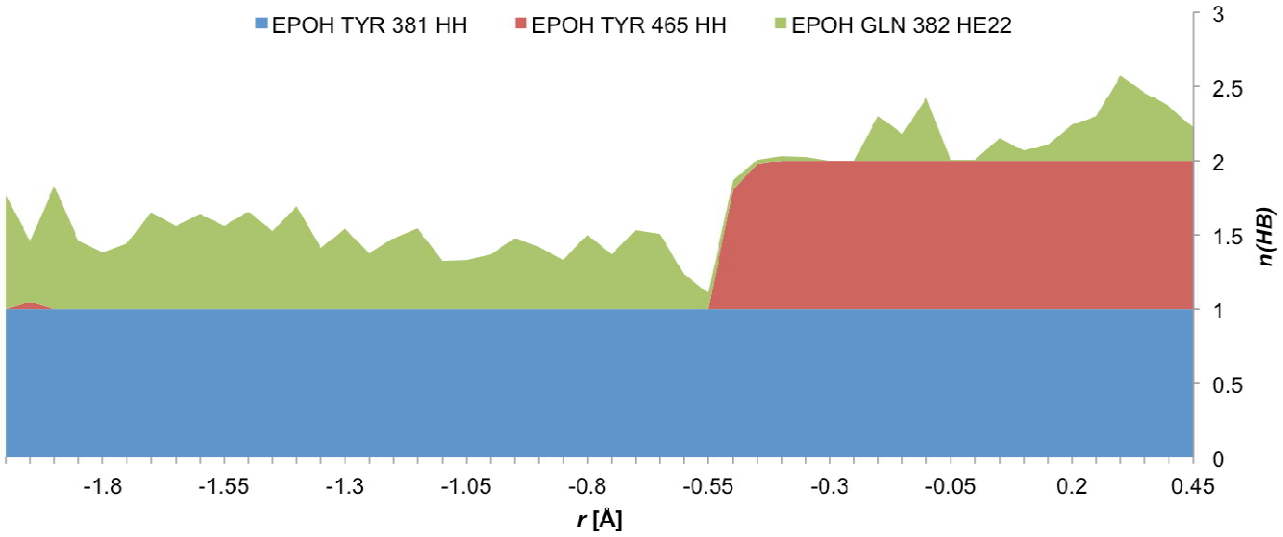


**K6: Hydrogen bonding to epoxide oxygen in extended AM1/CHARMM22 umbrella sampling MD simulations of ring opening at C(1) of t-SO (pathway 'f'):**

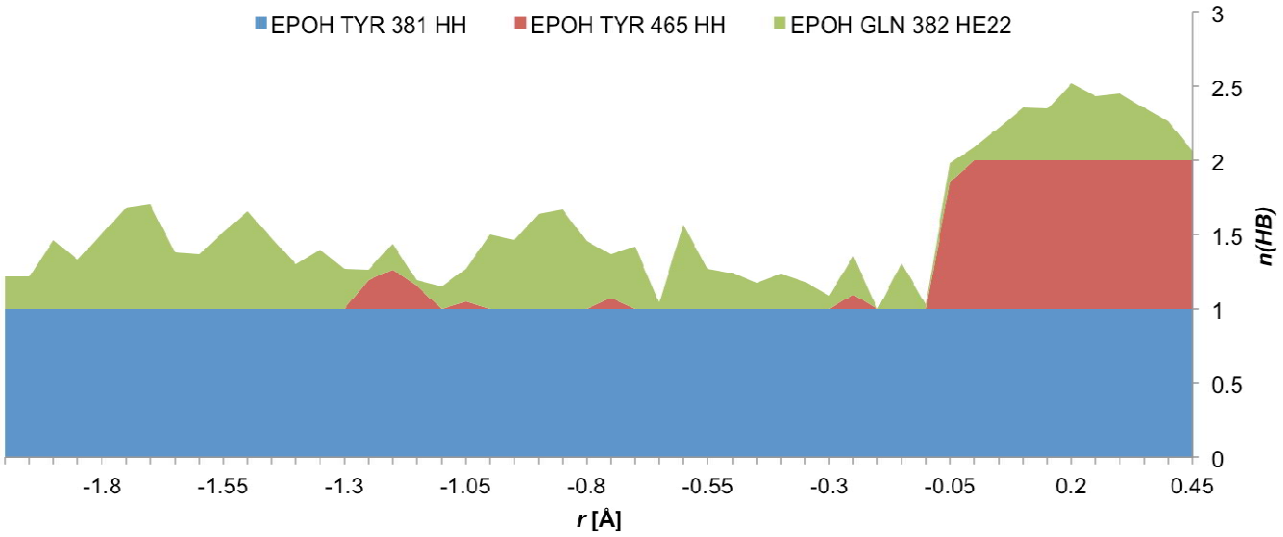

**K7: Hydrogen bonding to epoxide oxygen in extended AM1/CHARMM22 umbrella sampling MD simulations of ring opening at C(1) of t-SO (pathway 'g'):**

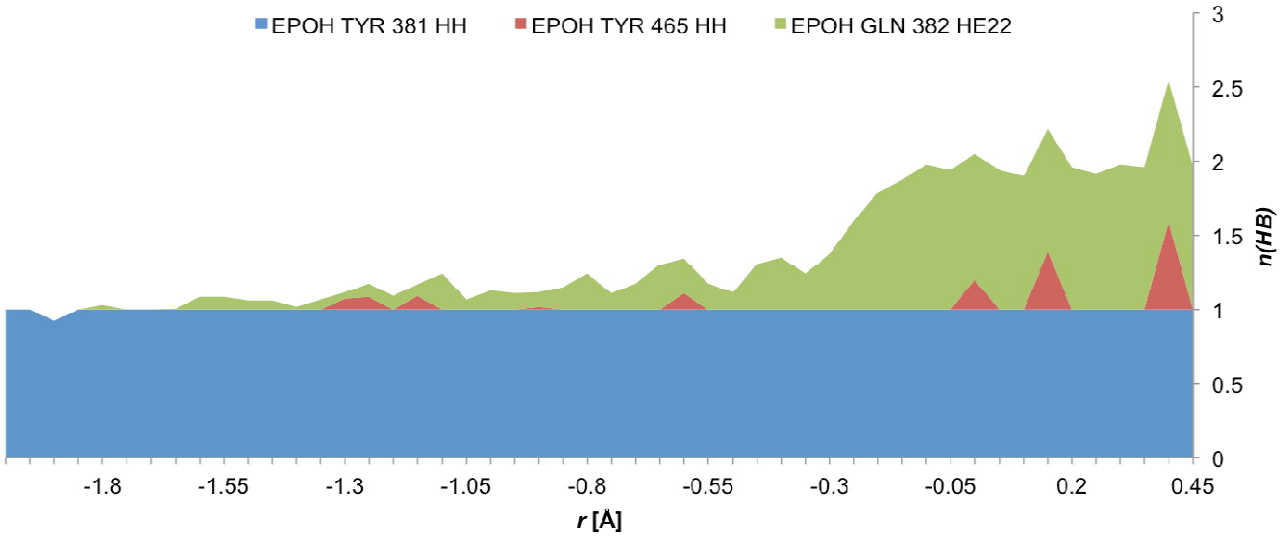


**K8: Hydrogen bonding to epoxide oxygen in extended AM1/CHARMM22 umbrella sampling MD simulations of ring opening at C(1) of t-SO (pathway 'h'):**

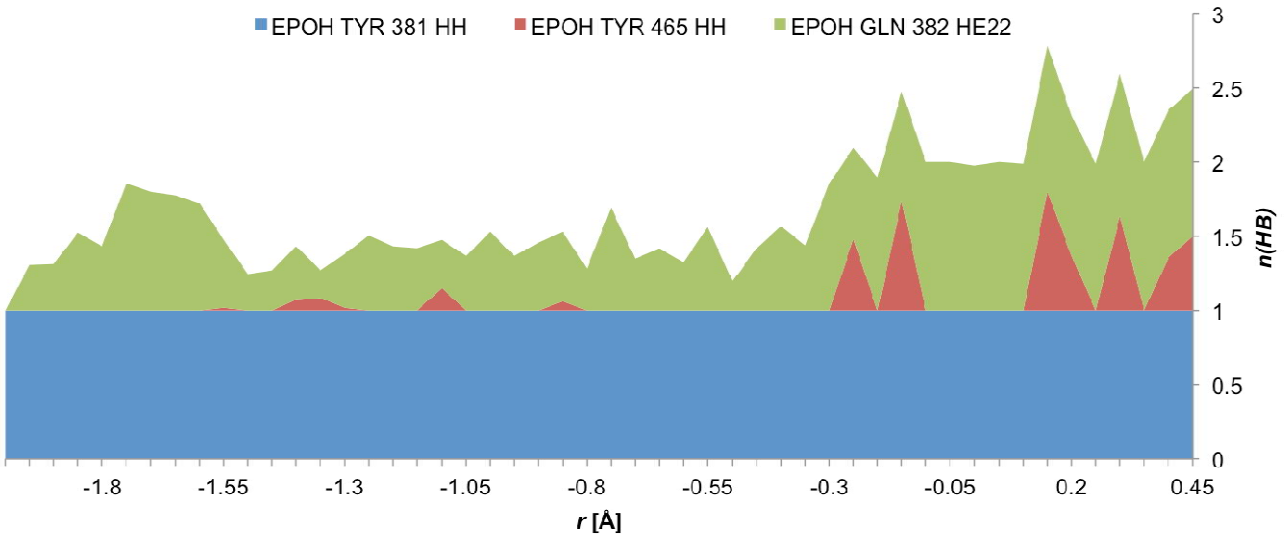

**K9: Hydrogen bonding to epoxide oxygen in extended AM1/CHARMM22 umbrella sampling MD simulations of ring opening at C(1) of t-SO (pathway 'i'):**

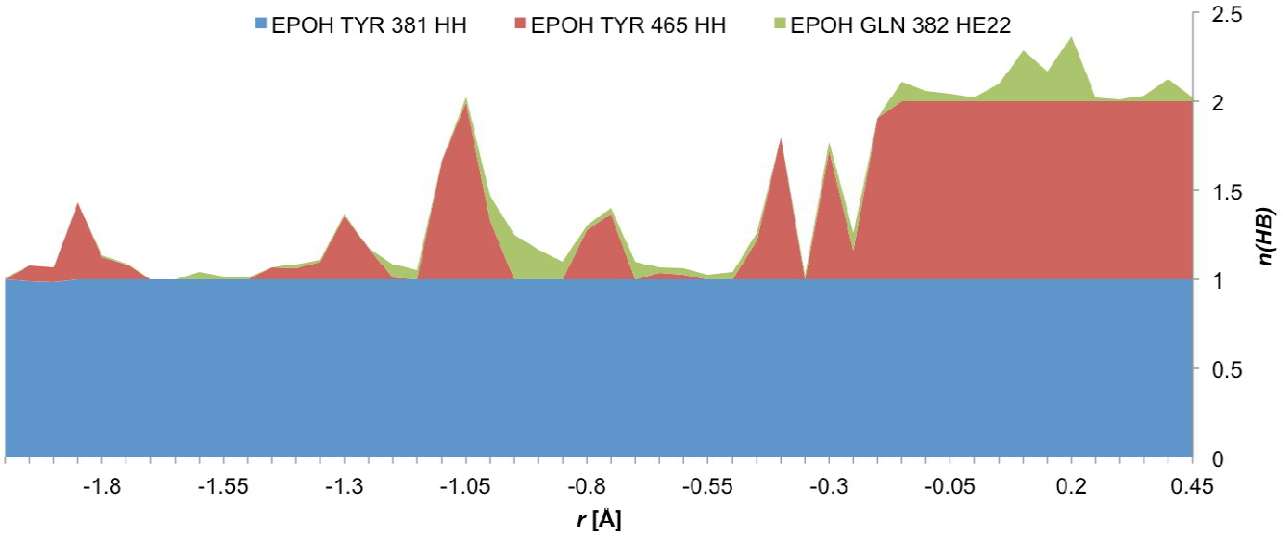


**K10: Hydrogen bonding to epoxide oxygen in extended AM1/CHARMM22 umbrella sampling MD simulations of ring opening at C(1) of t-SO (pathway 'j'):**

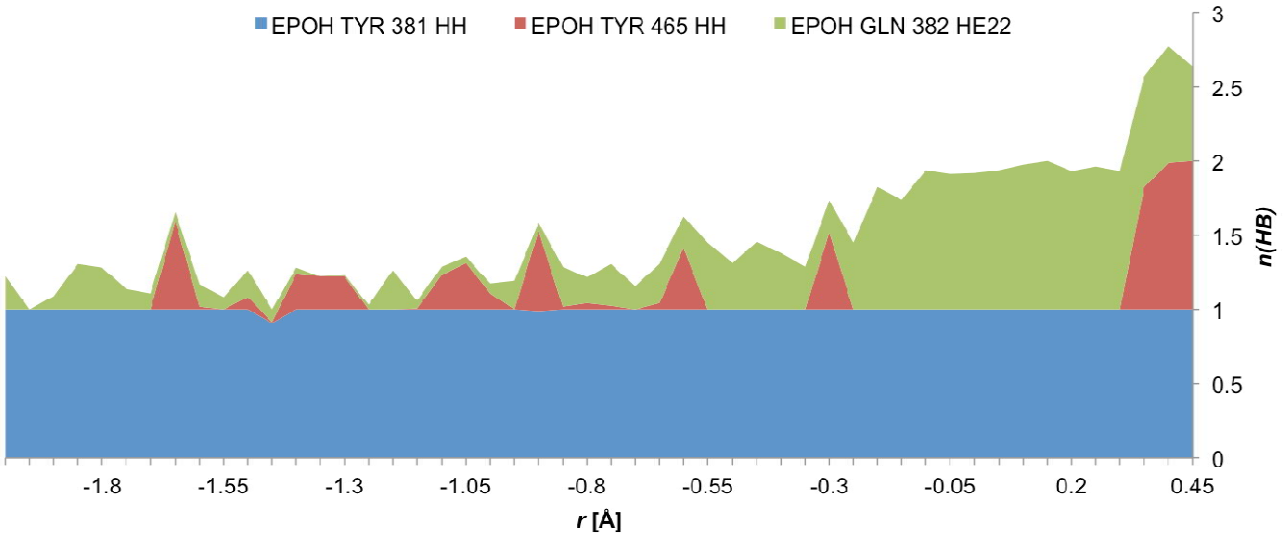

**K11: Hydrogen bonding to epoxide oxygen in extended AM1/CHARMM22 umbrella sampling MD simulations of ring opening at C(2) of t-SO (pathway 'a'):**

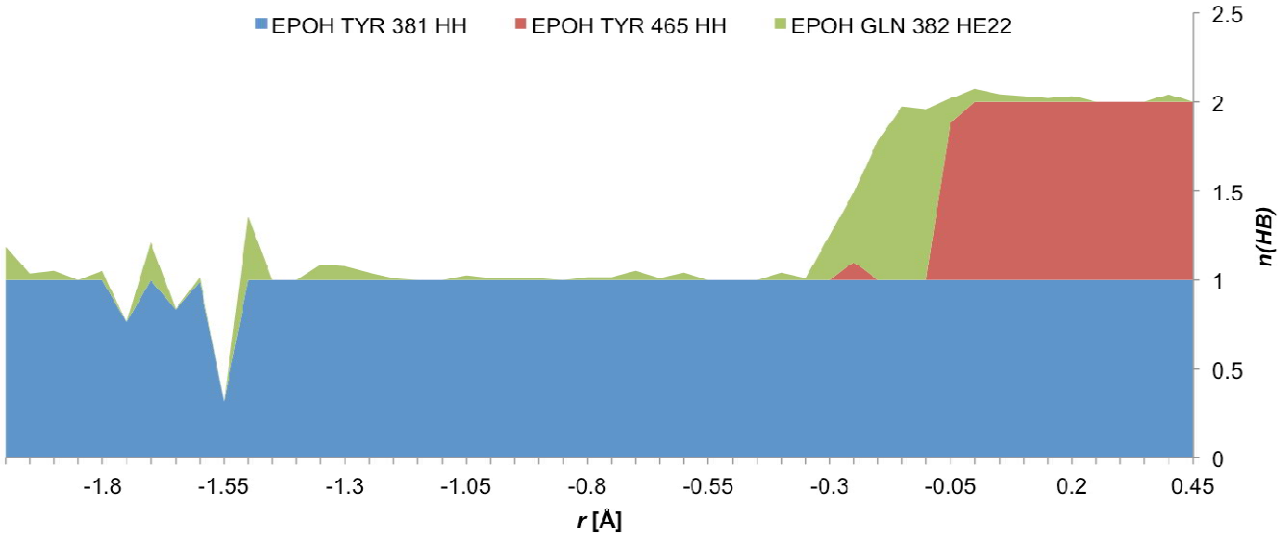


**K12: Hydrogen bonding to epoxide oxygen in extended AM1/CHARMM22 umbrella sampling MD simulations of ring opening at C(2) of t-SO (pathway 'b'):**

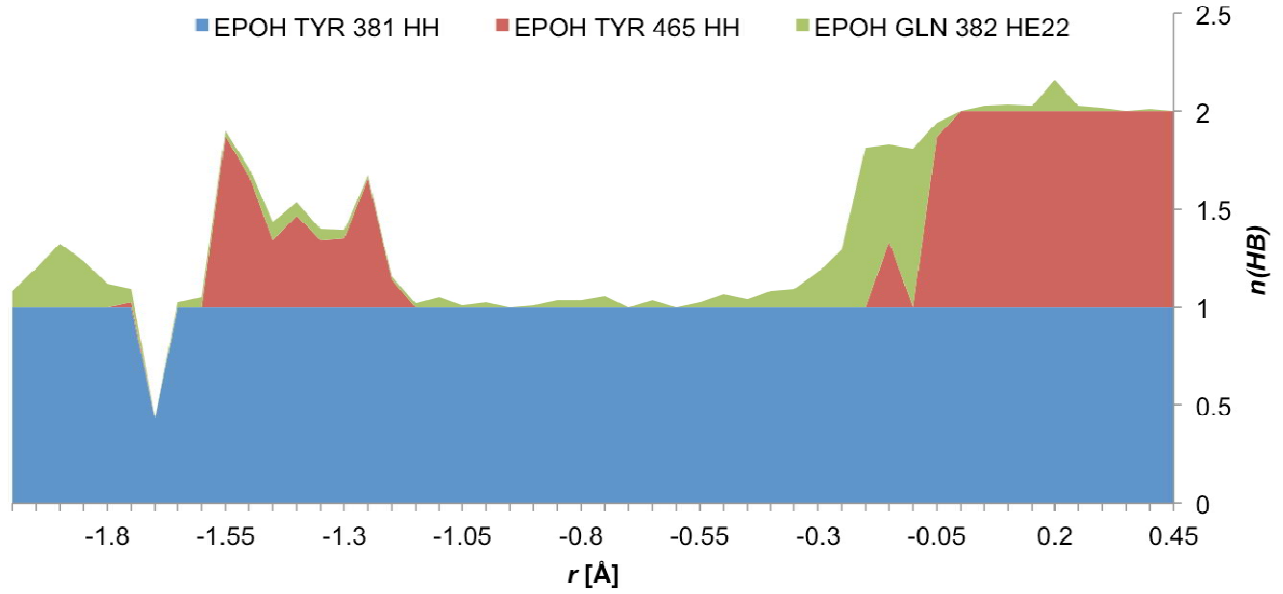

**K13: Hydrogen bonding to epoxide oxygen in extended AM1/CHARMM22 umbrella sampling MD simulations of ring opening at C(2) of t-SO (pathway 'c'):**

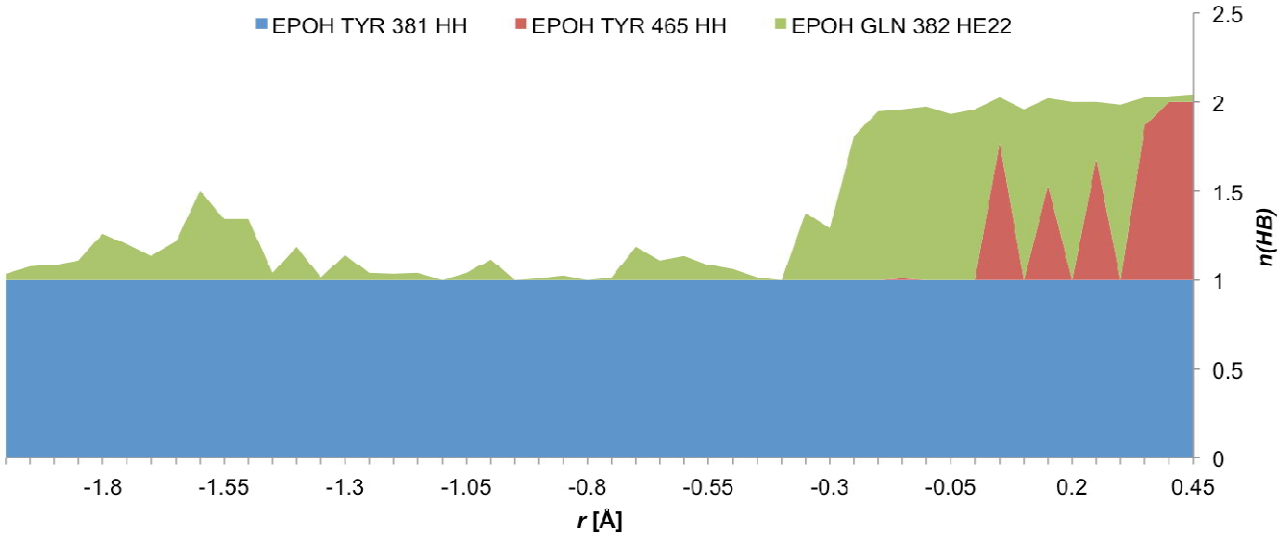


**K14: Hydrogen bonding to epoxide oxygen in extended AM1/CHARMM22 umbrella sampling MD simulations of ring opening at C(2) of t-SO (pathway 'e'):**

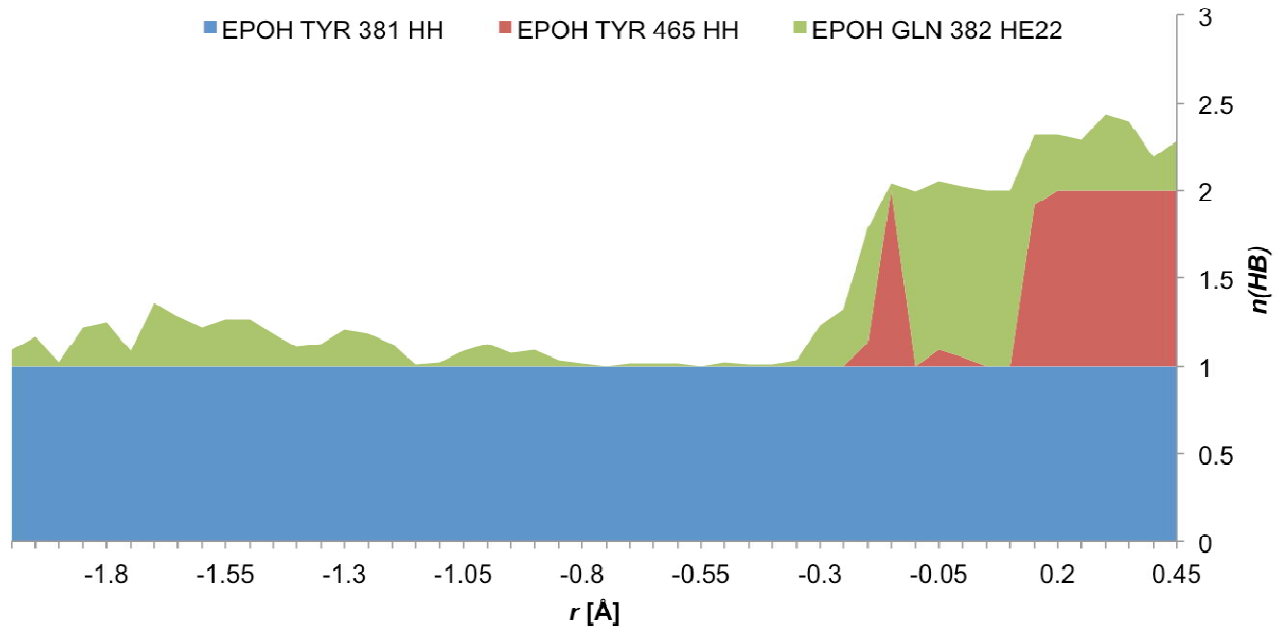

**K15: Hydrogen bonding to epoxide oxygen in extended AM1/CHARMM22 umbrella sampling MD simulations of ring opening at C(2) of t-SO (pathway 'f'):**

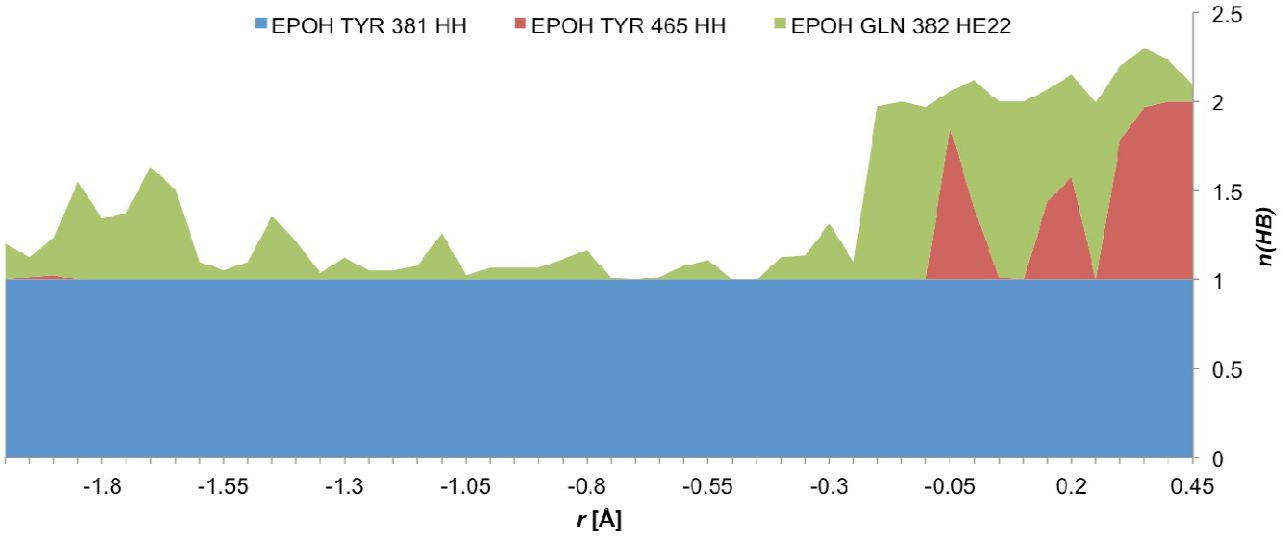


**K16: Hydrogen bonding to epoxide oxygen in extended AM1/CHARMM22 umbrella sampling MD simulations of ring opening at C(2) of t-SO (pathway 'g'):**

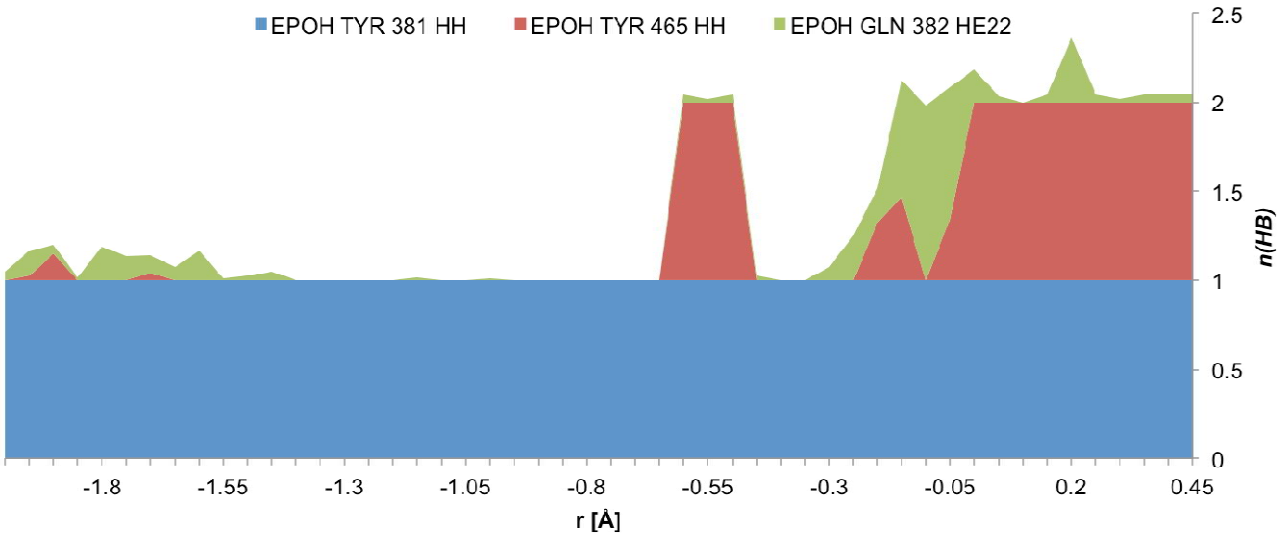

**K17: Hydrogen bonding to epoxide oxygen in extended AM1/CHARMM22 umbrella sampling MD simulations of ring opening at C(2) of t-SO (pathway 'h'):**

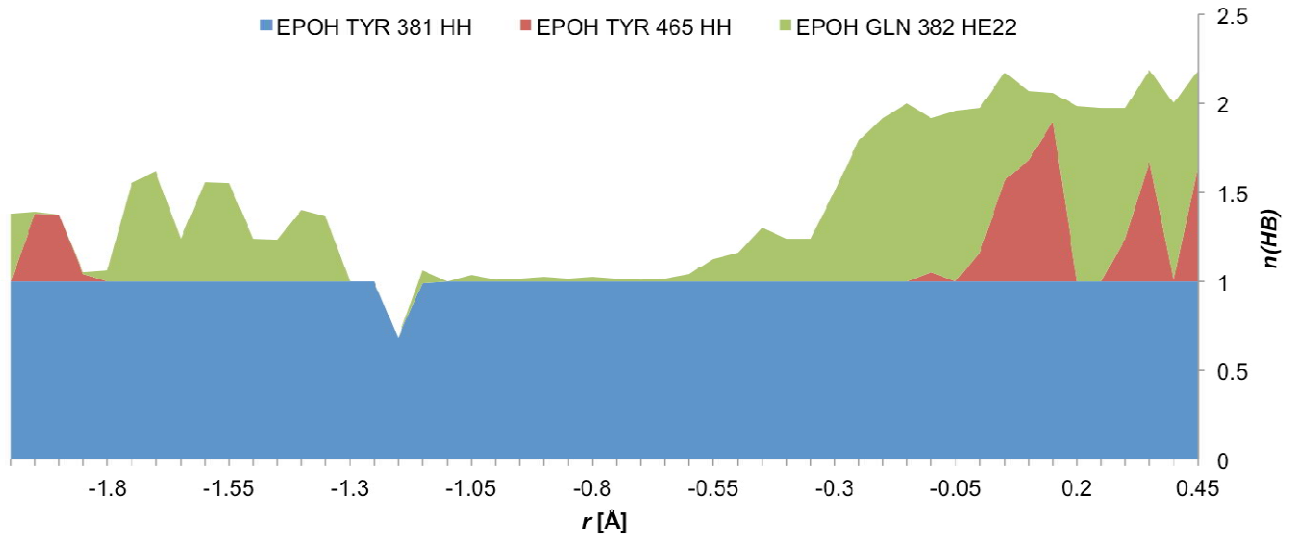


**K18: Hydrogen bonding to epoxide oxygen in extended AM1/CHARMM22 umbrella sampling MD simulations of ring opening at C(2) of t-SO (pathway 'i'):**

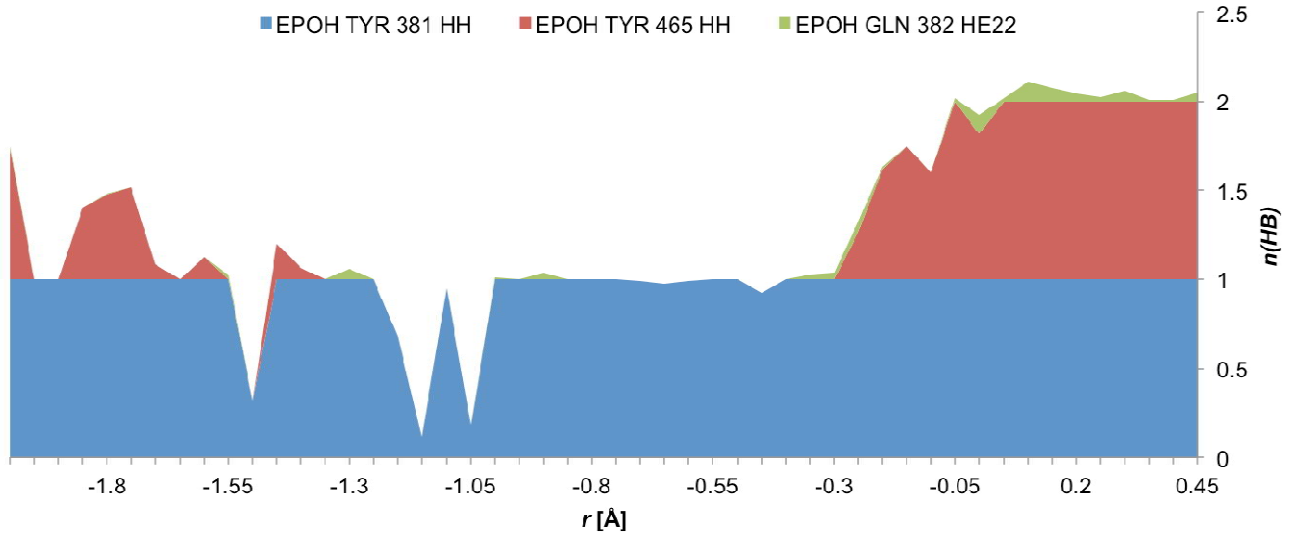

**K19: Hydrogen bonding to epoxide oxygen in extended AM1/CHARMM22 umbrella sampling MD simulations of ring opening at C(2) of t-SO (pathway 'j'):**

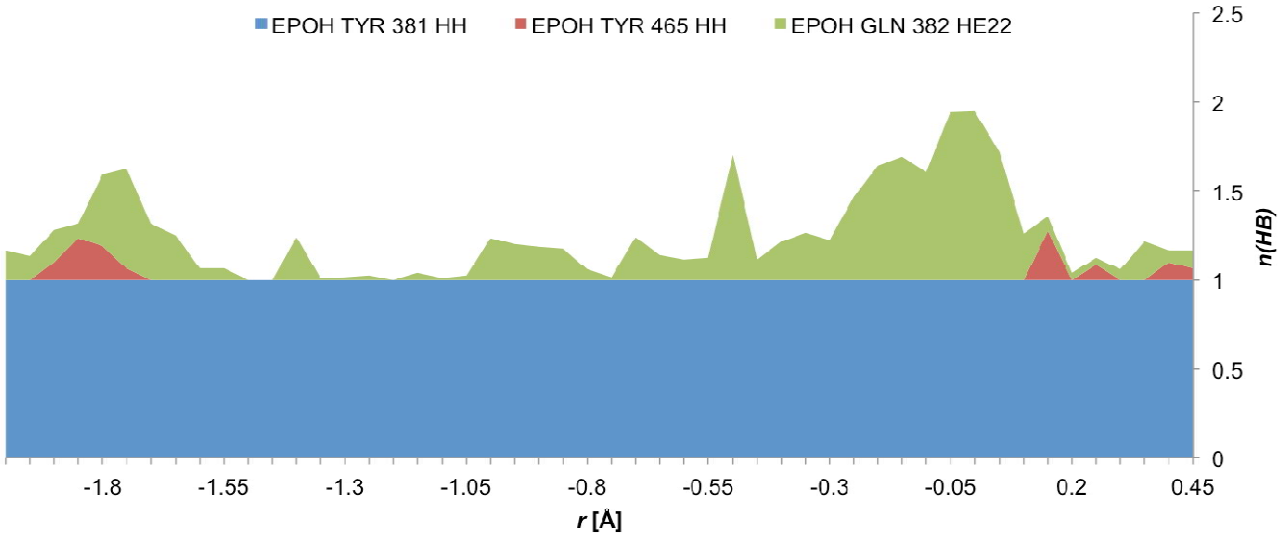

**Part L: Atomic charges from the AM1/CHARMM22 potential energy calculations**

**L1: Mulliken charges, taken as an average over all extended AM1/CHARMM22 umbrella sampling MD simulations, for nucleophilic ring opening at C(1) of t-SO. (C7 = epoxide C(1), O2 = epoxide oxygen, C15 = epoxide C(2), OD1 = Asp333 Oδ1, OD2 = Asp333 Oδ2)**

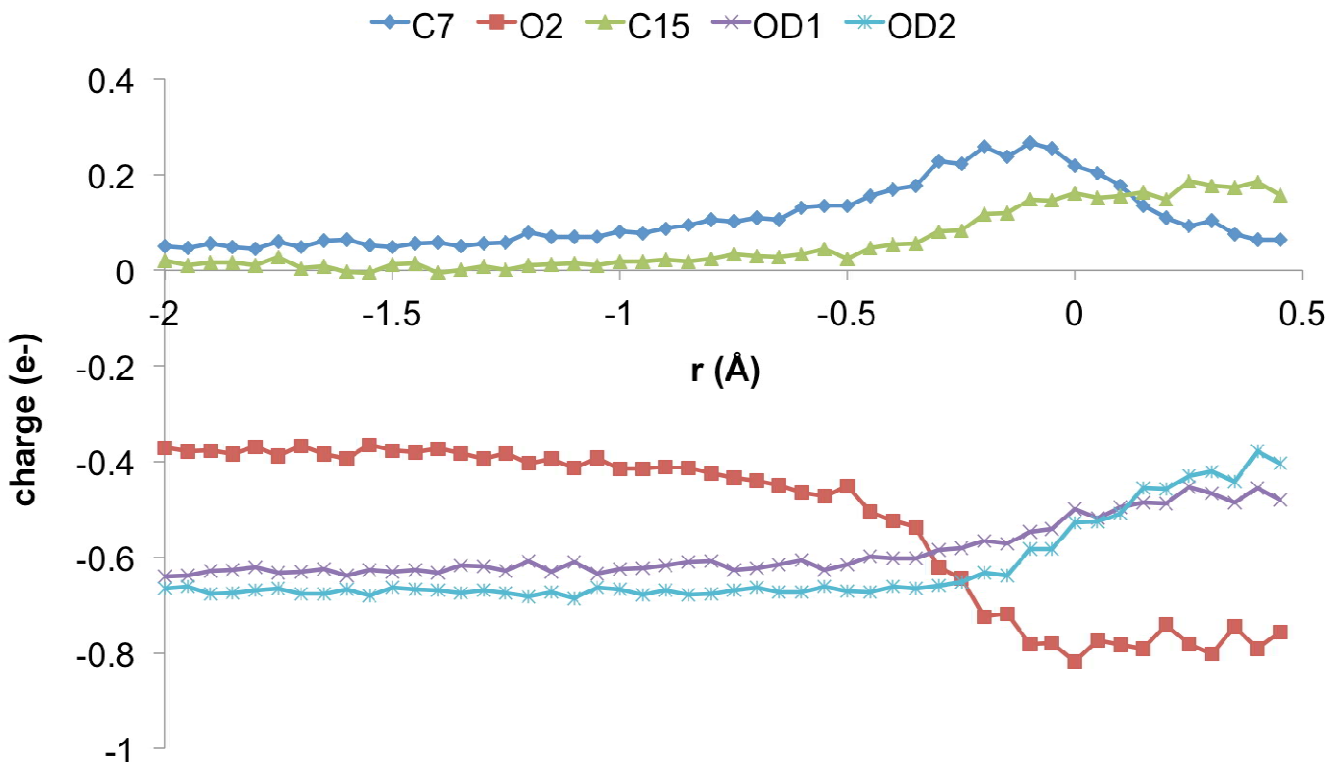

**L2: Mulliken charges, taken as an average over all extended AM1/CHARMM22 umbrella sampling MD simulations, for nucleophilic ring opening at C(2) of t-SO. (C7 = epoxide C(1), O2 = epoxide oxygen, C15 = epoxide C(2), OD1 = Asp333 Oδ1, OD2 = Asp333 Oδ2)**

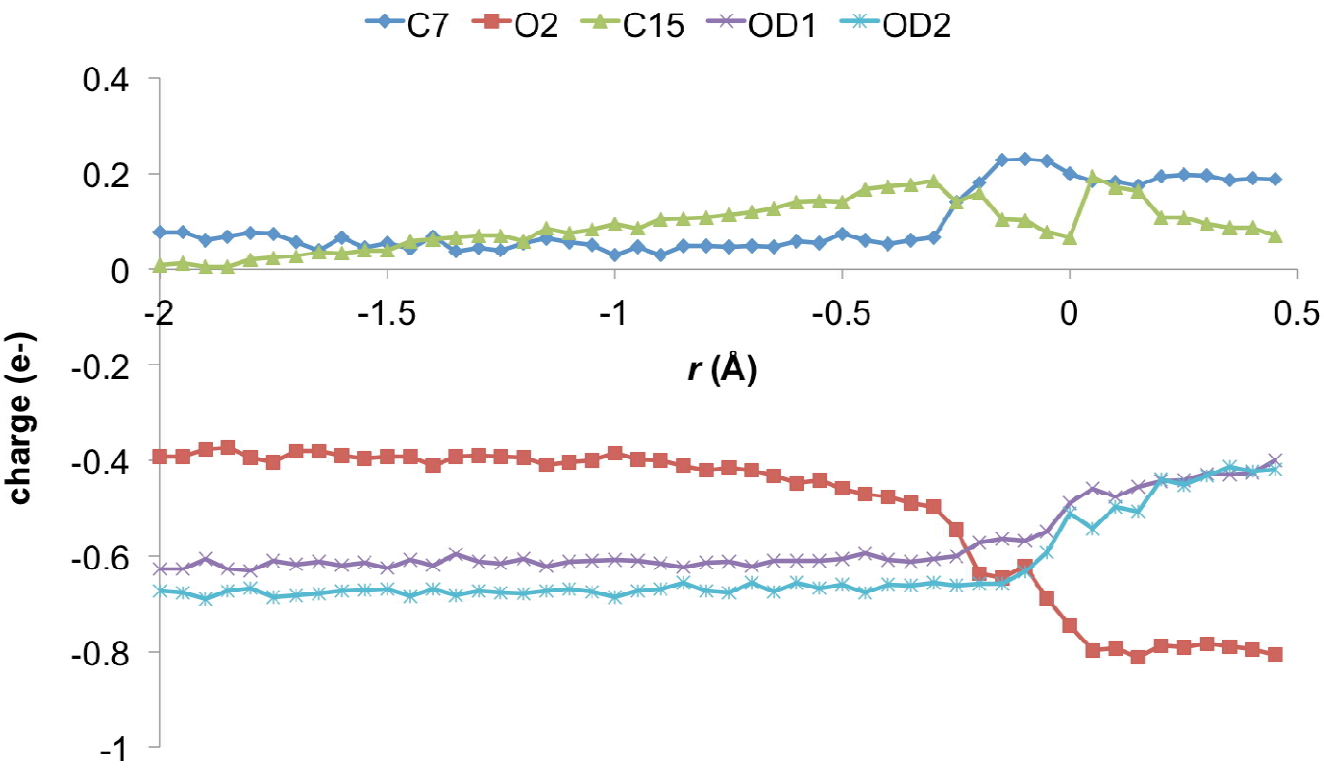

**L3: Mulliken charges, taken as an average over all extended AM1/CHARMM22 umbrella sampling MD simulations, for nucleophilic ring opening at C(1) of t-DPPO(1). (C7 = epoxide C(2), O2 = epoxide oxygen, C15 = epoxide C(1), OD1 = Asp333 Oδ1, OD2 = Asp333 Oδ2)**

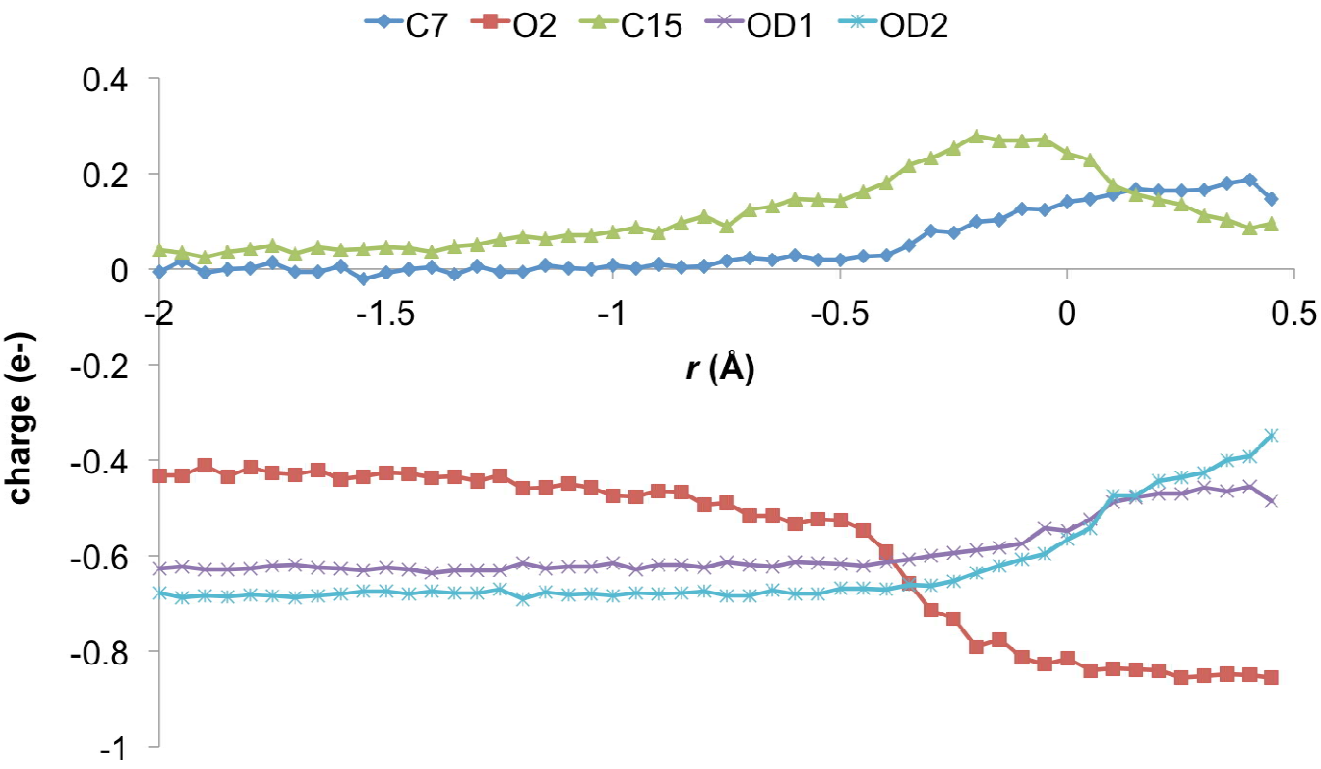

**L4: Mulliken charges, taken as an average over all extended AM1/CHARMM22 umbrella sampling MD simulations, for nucleophilic ring opening at C(2) of t-DPPO(1). (C7 = epoxide C(2), O2 = epoxide oxygen, C15 = epoxide C(1), OD1 = Asp333 Oδ1, OD2 = Asp333 Oδ2)**

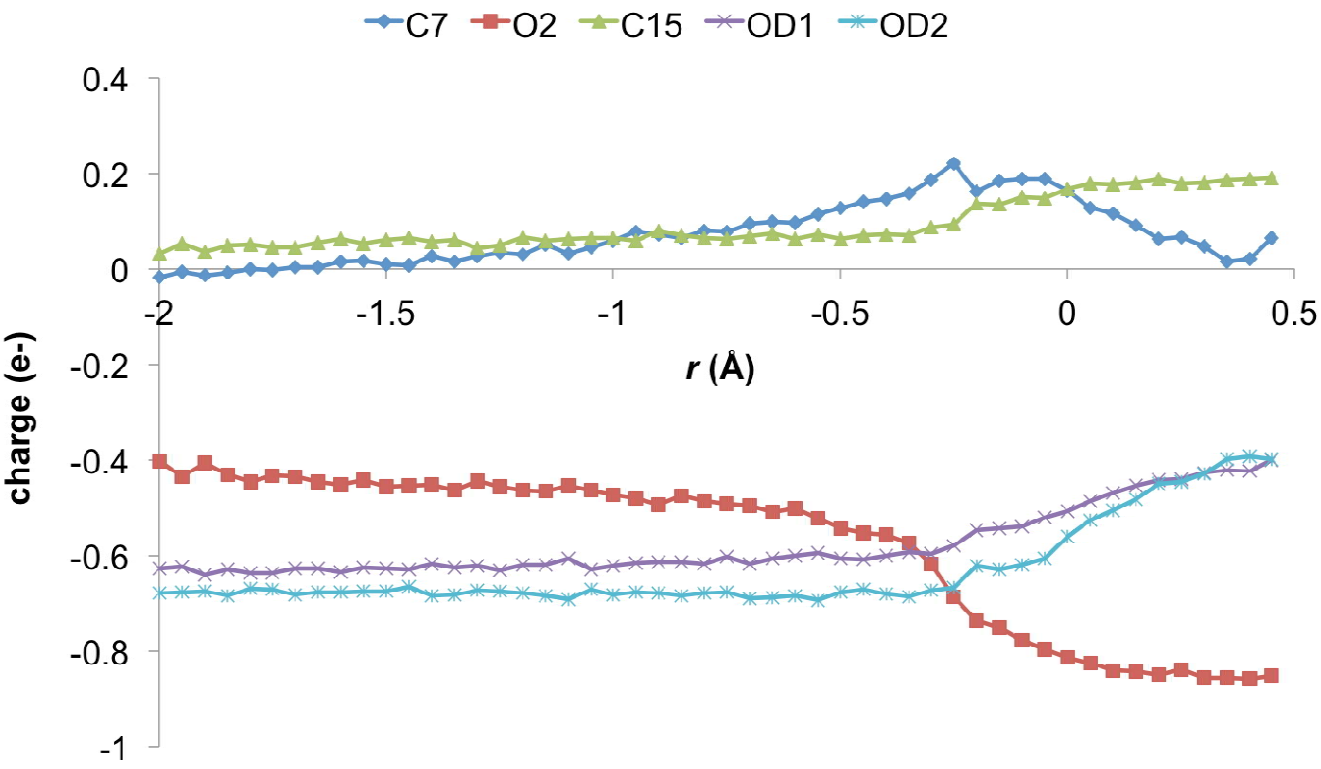

**L5: Mulliken charges, taken as an average over all extended AM1/CHARMM22 umbrella sampling MD simulations, for nucleophilic ring opening at C(1) of t-DPPO(2). (C7 = epoxide C(2), O2 = epoxide oxygen, C15 = epoxide C(1), OD1 = Asp333 Oδ1, OD2 = Asp333 Oδ2)**

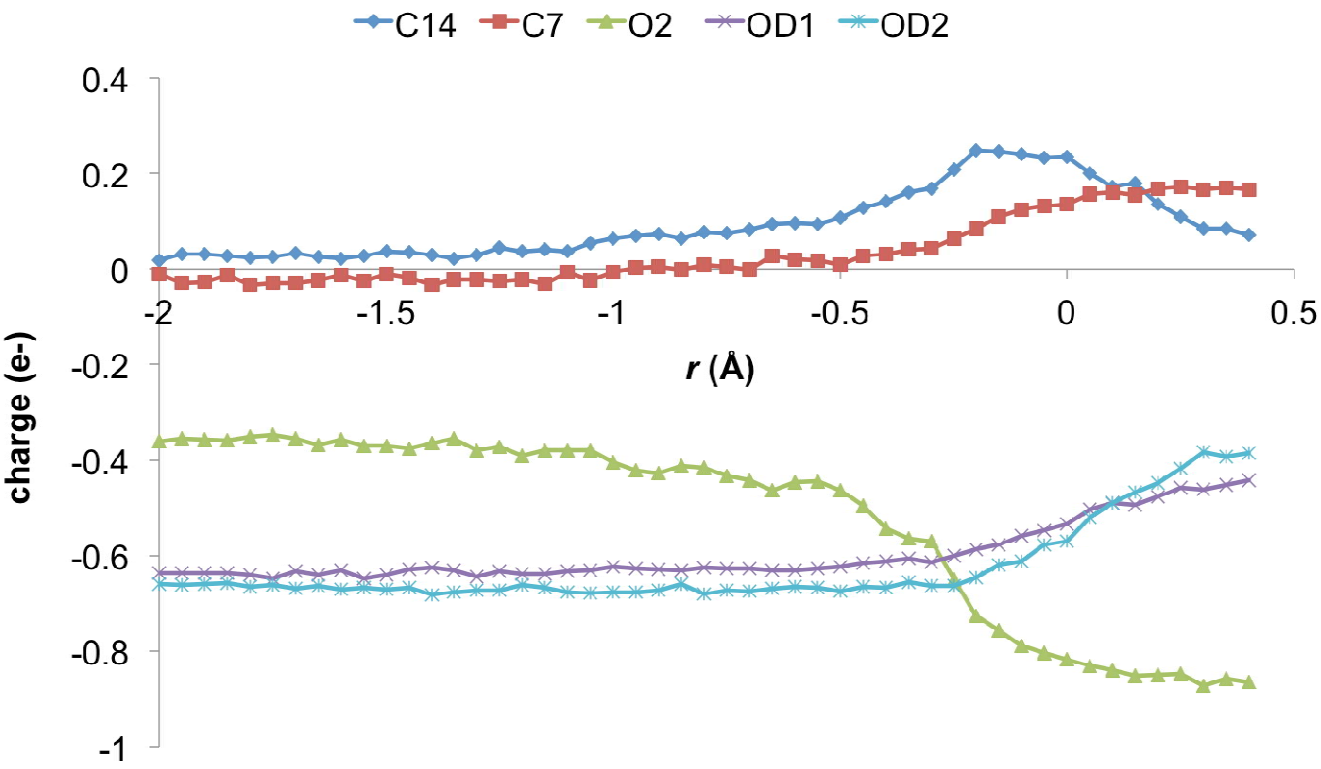

**L6: Mulliken charges, taken as an average over all extended AM1/CHARMM22 umbrella sampling MD simulations, for nucleophilic ring opening at C(2) of t-DPPO(2). (C7 = epoxide C(2), O2 = epoxide oxygen, C15 = epoxide C(1), OD1 = Asp333 Oδ1, OD2 = Asp333 Oδ2)**

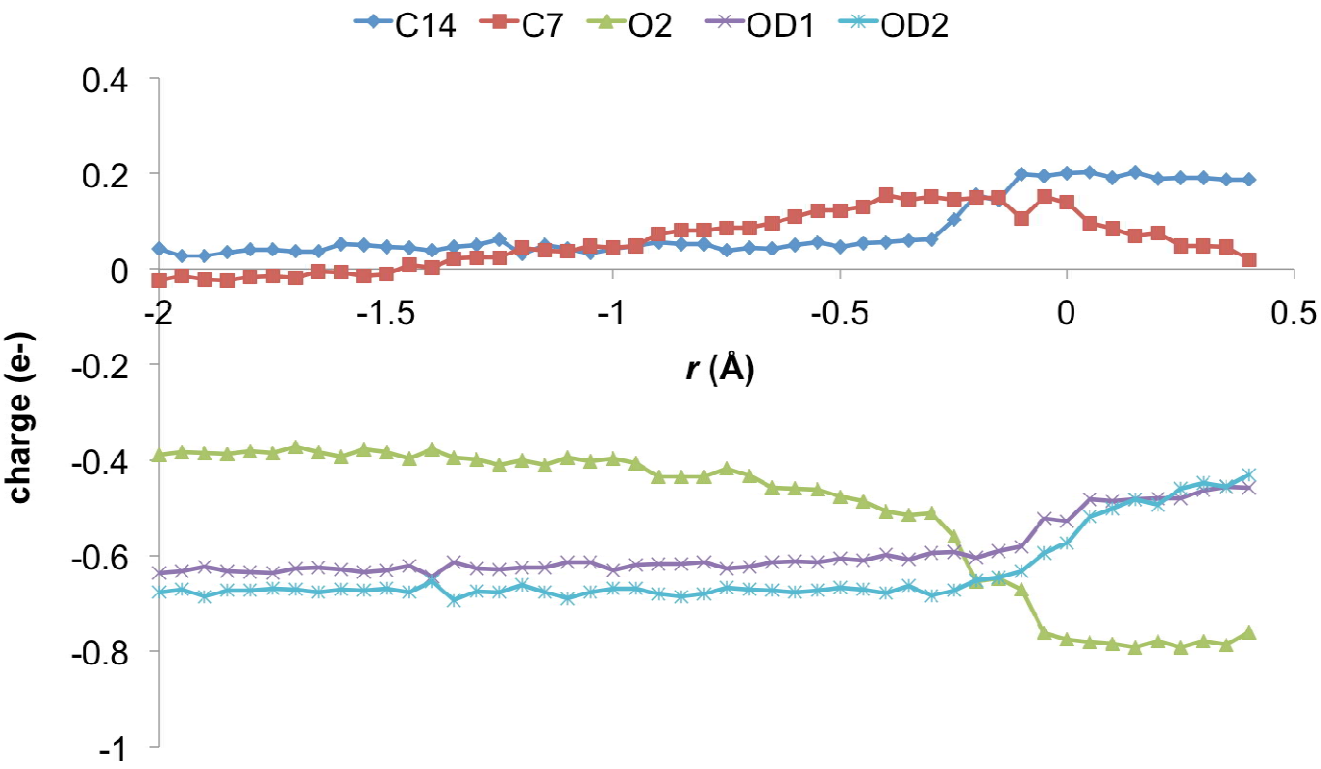

**Part M: Bond distances in transitions state geometries calculated from potential energy profiles.**

**M1: Bond distances (in Angstroms) for transition state geomertries calculated from AM1/CHARMM22 potential barriers for t-SO**

| Pathway | | AM1/CHARMM | | | | | |
|---|---|---|---|---|---|---|---|
| | | C1-O2 | C2-O2 | O2-Tyr465 | O2-Tyr381 | Asp333-C1 | Asp333-C2 |
| t-SO C(1) | a | 1.923 | 1.391 | 5.232 | 1.586 | 2.174 | 3.023 |
| | b | 1.893 | 1.395 | 1.664 | 1.598 | 2.193 | 3.092 |
| | c | 1.888 | 1.397 | 1.603 | 1.550 | 2.189 | 3.045 |
| | d | 1.879 | 1.398 | 1.699 | 1.618 | 2.179 | 3.034 |
| | e | 1.863 | 1.399 | 1.626 | 1.516 | 2.163 | 3.044 |
| | f | * | * | * | * | * | * |
| | g | 2.017 | 1.377 | 4.787 | 1.477 | 2.217 | 3.116 |
| | h | 1.994 | 1.379 | 5.034 | 1.532 | 2.195 | 3.074 |
| | i | 2.012 | 1.382 | 1.573 | 1.658 | 2.311 | 3.221 |
| | j | 2.000 | 1.380 | 4.649 | 1.502 | 2.200 | 3.101 |
| t-SO C(2) | a | 1.386 | 1.918 | 5.145 | 1.477 | 2.791 | 2.118 |
| | b | * | * | * | * | * | * |
| | c | 1.381 | 1.936 | 5.020 | 1.455 | 2.842 | 2.137 |
| | d | * | * | * | * | * | * |
| | e | 1.389 | 1.884 | 4.895 | 1.447 | 2.850 | 2.134 |
| | f | 1.383 | 1.924 | 4.888 | 1.451 | 2.816 | 2.123 |
| | g | 1.392 | 1.884 | 4.828 | 1.447 | 2.763 | 2.135 |
| | h | * | * | * | * | * | * |
| | i | * | * | * | * | * | * |
| | j | 1.391 | 1.885 | 4.378 | 1.462 | 2.803 | 2.136 |

* denotes pathways that did not converge

**M2: Bond distances (in Angstroms) for transition state geomertries calculated from B3LYP/CHARMM22 potential barriers for t-SO**

| Pathway | | B3LYP/CHARMM | | | | | |
|---|---|---|---|---|---|---|---|
| | | C1-O2 | C2-O2 | O2-Tyr465 | O2-Tyr381 | Asp333-C1 | Asp333-C2 |
| t-SO C(1) | a | 1.873 | 1.402 | 5.031 | 1.724 | 2.070 | 2.831 |
| | b | 1.794 | 1.420 | 1.770 | 1.703 | 2.193 | 2.915 |
| | c | 1.829 | 1.414 | 1.733 | 1.686 | 2.127 | 2.854 |
| | d | 1.791 | 1.421 | 1.776 | 1.697 | 2.189 | 2.894 |
| | e | 1.792 | 1.420 | 1.755 | 1.665 | 2.192 | 2.967 |
| | f | 1.857 | 1.408 | 3.856 | 1.714 | 2.156 | 2.963 |
| | g | 1.888 | 1.399 | 4.527 | 1.648 | 2.088 | 2.877 |
| | h | 1.879 | 1.406 | 4.699 | 1.687 | 2.078 | 2.855 |
| | i | 1.780 | 1.412 | 1.756 | 1.716 | 2.178 | 2.884 |
| | j | 1.880 | 1.400 | 4.353 | 1.669 | 2.079 | 2.858 |
| t-SO C(2) | a | 1.400 | 1.824 | 5.113 | 1.652 | 2.847 | 2.122 |
| | b | * | * | * | * | * | * |
| | c | 1.397 | 1.836 | 4.948 | 1.641 | 2.871 | 2.133 |
| | d | * | * | * | * | * | * |
| | e | 1.400 | 1.825 | 4.751 | 1.640 | 2.879 | 2.123 |
| | f | 1.389 | 1.881 | 4.822 | 1.647 | 2.866 | 2.077 |
| | g | 1.401 | 1.837 | 4.797 | 1.637 | 2.861 | 2.135 |
| | h | * | * | * | * | * | * |
| | i | * | * | * | * | * | * |
| | j | 1.411 | 1.768 | 4.427 | 1.651 | 2.871 | 2.167 |

* denotes pathways that did not converge

**M3: Bond distances (in Angstroms) for transition state geomertries calculated from AM1/CHARMM22 potential barriers for t-DPPO(1)**

| | | AM1/CHARMM | | | | | |
|---|---|---|---|---|---|---|---|
| | | C1-O2 | C2-O2 | O2-Tyr465 | O2-Tyr381 | Asp333-C1 | Asp333-C2 |
| t-DPPO1 C(1) | a | 1.936 | 1.388 | 1.558 | 1.526 | 2.136 | 2.824 |
| | b | 1.980 | 1.383 | 1.574 | 1.502 | 2.178 | 2.844 |
| | c | 1.958 | 1.387 | 1.576 | 1.558 | 2.158 | 2.848 |
| | d | 1.946 | 1.386 | 1.560 | 1.557 | 2.145 | 2.808 |
| | e | 1.925 | 1.391 | 1.585 | 1.500 | 2.125 | 2.799 |
| | f | 1.960 | 1.385 | 1.551 | 1.539 | 2.159 | 2.847 |
| | g | 1.914 | 1.391 | 1.559 | 1.564 | 2.165 | 2.859 |
| | h | 1.912 | 1.392 | 1.571 | 1.575 | 2.163 | 2.844 |
| | i | 1.972 | 1.383 | 1.541 | 1.578 | 2.172 | 2.843 |
| | j | 1.946 | 1.385 | 1.564 | 1.550 | 2.147 | 2.854 |
| t-DPPO1 C(2) | a | 1.391 | 1.933 | 1.592 | 1.561 | 2.998 | 2.182 |
| | b | 1.387 | 1.955 | 1.604 | 1.541 | 2.947 | 2.155 |
| | c | 1.399 | 1.884 | 1.630 | 1.617 | 2.999 | 2.184 |
| | d | 1.387 | 1.965 | 1.623 | 1.582 | 3.019 | 2.165 |
| | e | 1.387 | 1.966 | 1.606 | 1.556 | 3.021 | 2.165 |
| | f | 1.397 | 1.899 | 1.594 | 1.587 | 2.993 | 2.198 |
| | g | 1.385 | 1.977 | 1.611 | 1.567 | 3.033 | 2.176 |
| | h | 1.386 | 1.979 | 1.588 | 1.572 | 3.043 | 2.179 |
| | i | 1.382 | 2.002 | 1.602 | 1.542 | 3.101 | 2.203 |
| | j | * | * | * | * | * | * |

* denotes pathways that did not converge

**M4: Bond distances (in Angstroms) for transition state geomertries calculated from B3LYP/CHARMM22 potential barriers for t-DPPO(1)**

| | | B3LYP/CHARMM | | | | | |
|---|---|---|---|---|---|---|---|
| | | C1-O2 | C2-O2 | O2-Tyr465 | O2-Tyr381 | Asp333-C1 | Asp333-C2 |
| t-DPPO1 C(1) | a | 1.866 | 1.403 | 1.714 | 1.678 | 2.163 | 2.866 |
| | b | 1.884 | 1.399 | 1.709 | 1.660 | 2.179 | 2.835 |
| | c | 1.835 | 1.408 | 1.707 | 1.673 | 2.233 | 2.840 |
| | d | 1.879 | 1.400 | 1.711 | 1.691 | 2.177 | 2.867 |
| | e | 1.899 | 1.403 | 1.712 | 1.657 | 2.096 | 2.827 |
| | f | 1.919 | 1.395 | 1.699 | 1.678 | 2.116 | 2.840 |
| | g | 1.868 | 1.405 | 1.700 | 1.689 | 2.167 | 2.855 |
| | h | 1.863 | 1.404 | 1.708 | 1.692 | 2.162 | 2.854 |
| | i | 1.880 | 1.402 | 1.706 | 1.702 | 2.179 | 2.838 |
| | j | 1.866 | 1.403 | 1.713 | 1.690 | 2.165 | 2.857 |
| t-DPPO1 C(2) | a | 1.408 | 1.895 | 1.705 | 1.706 | 2.891 | 2.093 |
| | b | 1.417 | 1.820 | 1.740 | 1.702 | 2.875 | 2.119 |
| | c | 1.411 | 1.889 | 1.701 | 1.720 | 2.925 | 2.087 |
| | d | 1.410 | 1.891 | 1.718 | 1.724 | 2.924 | 2.092 |
| | e | 1.411 | 1.890 | 1.712 | 1.708 | 2.927 | 2.089 |
| | f | 1.409 | 1.900 | 1.689 | 1.715 | 2.915 | 2.099 |
| | g | 1.408 | 1.896 | 1.720 | 1.724 | 2.922 | 2.095 |
| | h | 1.410 | 1.893 | 1.717 | 1.732 | 2.945 | 2.091 |
| | i | 1.408 | 1.914 | 1.732 | 1.713 | 2.995 | 2.112 |
| | j | * | * | * | * | * | * |

* denotes pathways that did not converge

**M5: Bond distances (in Angstroms) for transition state geomertries calculated from AM1/CHARMM22 potential barriers for t-DPPO(2)**

| | | AM1/CHARMM | | | | | |
|---|---|---|---|---|---|---|---|
| | | C1-O2 | C2-O2 | O2-Tyr465 | O2-Tyr381 | Asp333-C1 | Asp333-C2 |
| t-DPPO2 C(1) | a | 2.049 | 1.367 | 4.622 | 1.521 | 2.148 | 2.963 |
| | b | 2.049 | 1.367 | 4.622 | 1.521 | 2.148 | 2.963 |
| | c | 1.966 | 1.383 | 1.563 | 1.545 | 2.265 | 3.088 |
| | d | 1.926 | 1.387 | 1.568 | 1.663 | 2.226 | 3.038 |
| | e | 1.842 | 1.397 | 1.604 | 1.586 | 2.193 | 2.939 |
| | f | 1.832 | 1.399 | 1.625 | 1.603 | 2.183 | 2.926 |
| | g | 2.111 | 1.364 | 5.387 | 1.487 | 2.163 | 3.054 |
| | h | 1.965 | 1.380 | 1.633 | 1.603 | 2.216 | 3.042 |
| | i | 1.872 | 1.394 | 1.618 | 1.600 | 2.222 | 2.972 |
| | j | 1.916 | 1.388 | 1.609 | 1.561 | 2.216 | 2.944 |
| t-DPPO2 C(2) | a | 1.378 | 1.948 | 4.817 | 1.474 | 2.805 | 2.047 |
| | b | 1.366 | 2.011 | 4.824 | 1.456 | 2.918 | 2.012 |
| | c | * | * | * | * | * | * |
| | d | 1.376 | 1.963 | 4.839 | 1.469 | 2.960 | 2.063 |
| | e | 1.400 | 1.804 | 4.834 | 1.517 | 2.934 | 2.107 |
| | f | 1.370 | 1.990 | 4.833 | 1.461 | 2.943 | 2.040 |
| | g | * | * | * | * | * | * |
| | h | 1.393 | 1.850 | 4.839 | 1.502 | 2.954 | 2.103 |
| | i | 1.376 | 1.963 | 4.839 | 1.469 | 2.960 | 2.063 |
| | j | * | * | * | * | * | * |

* denotes pathways that did not converge

**M6: Bond distances (in Angstroms) for transition state geomertries calculated from B3LYP/CHARMM22 potential barriers for t-DPPO(2)**

| | | B3LYP/CHARMM | | | | | |
|---|---|---|---|---|---|---|---|
| | | C1-O2 | C2-O2 | O2-Tyr465 | O2-Tyr381 | Asp333-C1 | Asp333-C2 |
| t-DPPO2 C(1) | a | 1.846 | 1.413 | 4.490 | 1.687 | 2.148 | 2.810 |
| | b | 1.907 | 1.403 | 4.530 | 1.687 | 2.107 | 2.807 |
| | c | 1.869 | 1.405 | 1.728 | 1.688 | 2.168 | 2.842 |
| | d | 1.820 | 1.415 | 1.724 | 1.748 | 2.220 | 2.847 |
| | e | 1.861 | 1.403 | 1.746 | 1.679 | 2.160 | 2.843 |
| | f | 1.819 | 1.412 | 1.733 | 1.696 | 2.218 | 2.862 |
| | g | 1.930 | 1.405 | 5.069 | 1.685 | 2.131 | 2.840 |
| | h | 1.859 | 1.409 | 1.770 | 1.725 | 2.159 | 2.867 |
| | i | 1.887 | 1.400 | 1.740 | 1.693 | 2.186 | 2.861 |
| | j | 1.864 | 1.406 | 1.744 | 1.687 | 2.162 | 2.816 |
| t-DPPO2 C(2) | a | 1.399 | 1.861 | 4.652 | 1.687 | 2.866 | 2.059 |
| | b | 1.388 | 1.872 | 4.641 | 1.689 | 2.993 | 2.075 |
| | c | 1.414 | 1.836 | 1.774 | 1.678 | 2.837 | 2.135 |
| | d | 1.400 | 1.820 | 4.160 | 1.714 | 2.864 | 2.122 |
| | e | 1.414 | 1.818 | 1.752 | 1.693 | 2.840 | 2.116 |
| | f | 1.391 | 1.851 | 4.336 | 1.690 | 2.842 | 2.052 |
| | g | * | * | * | * | * | * |
| | h | 1.411 | 1.851 | 1.750 | 1.717 | 2.878 | 2.150 |
| | i | 1.393 | 1.888 | 4.277 | 1.674 | 2.861 | 2.088 |
| | j | * | * | * | * | * | * |

* denotes pathways that did not converge